

1 **Drainage evolution and exhumation history of the eastern Himalaya:**

2 **Insights from the Nicobar Fan, northeastern Indian Ocean**

3 **Wen-Huang Chen^{1,2,3*}, Yi Yan^{1*}, Peter D. Clift⁴, Andrew Carter⁵, Chi-Yue Huang⁶,**
4 **Kevin T. Pickering⁷, Farid Chemale Jr.⁸, Yehua Shan¹, and Xinchang Zhang¹**

5 ¹Key Laboratory of Ocean and Marginal Sea Geology, Guangzhou Institute of
6 Geochemistry, Chinese Academy of Sciences, Guangzhou 510640, China

7 ²Southern Marine Science and Engineering Guangdong Laboratory (Guangzhou),
8 Guangzhou 511458, China

9 ³Innovation Academy of South China Sea Ecology and Environmental Engineering,
10 Chinese Academy of Sciences, Guangzhou, 510640, China

11 ⁴Department of Geology and Geophysics, Louisiana State University, Baton Rouge, LA
12 70803, USA

13 ⁵Department of Earth and Planetary Sciences, Birkbeck, University of London, Malet
14 Street, London WC1E 7HX, United Kingdom

15 ⁶School of Ocean and Earth Science, Tongji University, Shanghai 200092, China

16 ⁷Department of Earth Sciences, University College London (UCL), London WC1E 6BT,
17 United Kingdom

18 ⁸Programa de Pós-Graduação em Geologia, Universidade do Vale do Rio dos Sinos,
19 93.022-750 São Leopoldo, RS, Brazil

20 *Corresponding Authors: Wen-Huang Chen, chenwenhuang@gig.ac.cn, and Yi Yan,
21 yanyi@gig.ac.cn

22

23 **Abstract**

24 The eastern Himalayan syntaxis, where the Yarlung Tsangpo sharply bends, is one of the
25 areas experiencing most rapid exhumation on Earth. The rapid exhumation is often
26 regarded as the result of capture of the Yarlung Tsangpo by the Brahmaputra River.
27 However, both the timing of integration of the Yarlung Tsangpo-Brahmaputra River and
28 initiation of the rapid syntaxial exhumation are debated. As the ultimate sedimentary trap
29 of the Yarlung Tsangpo-Brahmaputra River, the Nicobar Fan is a window to look into the
30 drainage evolution and exhumation history of the eastern Himalaya. International Ocean
31 Discovery Program Expedition 362 drilled the Nicobar Fan for the first time, recovering
32 fan sediments dating back to the Early Miocene (~19 Ma). We apply trace elements and
33 Sr-Nd isotopes to investigate the provenance of the sediments in the Nicobar Fan with the
34 aim of constraining the timing of integration of the Yarlung Tsangpo-Brahmaputra River
35 and initiation of the rapid syntaxial exhumation. The geochemical and Sr-Nd isotope
36 compositions indicate an eastern Himalayan source dominated by the Greater Himalaya,
37 with significant Gangdese arc contribution and primarily carried by the Brahmaputra River.
38 Flux of Gangdese arc material appears to have been continuous from the base of the
39 Nicobar Fan, suggesting that the Yarlung Tsangpo-Brahmaputra River has been established
40 at least since ~19 Ma. Synchronously with the sharp rise in sedimentation rate, the abrupt
41 change of geochemical and isotope compositions at ~9.2 Ma indicates an increase in
42 erosion of the Greater Himalaya as the result of initiation of rapid exhumation in the broad

43 syntaxial region. The proportion of Greater Himalayan material increased again at 3.5–1.7
44 Ma, consistent with a younger pulse of rapid exhumation focused in the core of the syntaxis
45 since ~3.5 Ma. Our results show that initiation of the rapid syntaxial exhumation postdated
46 integration of the Yarlung Tsangpo-Brahmaputra River by at least ~10 m.y. Therefore,
47 tectonic uplift rather than river capture could be responsible for the initiation of the rapid
48 syntaxial exhumation.

49 *Key words:* Nicobar Fan, Yarlung Tsangpo-Brahmaputra River, eastern Himalayan
50 syntaxis, sedimentary record, International Ocean Discovery Program Expedition 362

51

52 **1. Introduction**

53 Collisional tectonics induces topographic variation and results in drainage
54 reorganization via mechanisms such as river capture, diversion and reversal (e.g.
55 Brookfield, 1998; Clark et al., 2004). Drainage reorganization markedly affects the
56 distribution and intensity of erosion over an orogen, which in turn influences the style and
57 location of crustal deformation (Cina et al., 2009). Therefore, study of drainage evolution
58 during collisional orogeny is crucial to understanding the complex interplay between
59 tectonic deformation and surface erosion (e.g. Bracciali et al., 2015). The Himalayan
60 orogen, where active collision is ongoing and major South Asian rivers originate, is an
61 ideal place in which to recognize tectonic-erosion interactions. The eastern Himalayan
62 syntaxis is one of the most active tectonic regions on Earth and characterized by very rapid
63 rock uplift and exhumation (Burg et al., 1997; Ding et al., 2001) (Fig. 1). The Yarlung
64 Tsangpo runs eastward along the suture between the Himalaya and the Lhasa block, and
65 then sharply bends southward through the eastern syntaxis, carving one of the world's

66 largest and deepest gorges, the Yarlung Tsangpo Gorge. Downstream of the gorge, the
67 Yarlung Tsangpo is called the Siang River and becomes the southwestward-flowing
68 Brahmaputra River in the Himalayan foreland. It then meets the Ganges River, and finally
69 discharges into the Bay of Bengal and the northeastern Indian Ocean, where it accumulates
70 as the Bengal-Nicobar Fan system (Fig. 1). The sediments are now transferred to the
71 Bengal Fan by turbidite currents via the Swatch-of-No-Ground submarine canyon and the
72 Active Channel (Fig. 1) which has been active since 12.5 ka BP, however, there were
73 probably more than one canyon-channel system at times before then (Curry et al., 2003).
74 The Bengal-Nicobar Fan system extends southward for over 3000 km to $\sim 7^{\circ}\text{S}$ and covers
75 an area of $\sim 4 \times 10^6 \text{ km}^2$ with a volume of $> 8 \times 10^6 \text{ km}^3$ since ca. 20 Ma (Curry et al., 2003,
76 Pickering et al., 2020). As the ultimate sediment trap of the Ganges River and Yarlung
77 Tsangpo-Brahmaputra River, the Bengal-Nicobar Fan preserves records of Himalayan
78 erosion and is therefore vital to deciphering the drainage evolution and exhumation history
79 of the eastern Himalaya.

80 The eastern Himalayan syntaxis presently feeds 45–70% of the bulk sediment flux of
81 the Brahmaputra River, suggesting an exhumation rate up to 10 mm/yr or more (e.g. Singh
82 and France-Lanord, 2002; Bracciali et al., 2016). Such high exhumation rates are also
83 supported by the bedrock cooling age as young as $< 1 \text{ Ma}$ (e.g. Seward and Burg, 2008).
84 To explain the extremely rapid syntaxial exhumation, most researchers emphasize the role
85 of tectonics caused by northward indentation of the northeastern corner of the Indian plate
86 into Eurasia, which leads to growth of the syntaxis (e.g. Burg et al., 1997; Seward and Burg,
87 2008; Bendick and Ehlers, 2014). However, the “tectonic aneurysm” model highlights the
88 potential coupling between tectonics and erosion and associates the rapid exhumation with

89 the incision of the Yarlung Tsangpo Gorge (Zeitler et al., 2001, 2014). This model suggests
90 that rapid, focused erosion weakens the upper crust, leading to lower crustal flow into the
91 weakened zone, and promoting the doming of the upper crust, thus generating a self-
92 sustaining feedback between tectonic deformation and surface erosion (Zeitler et al., 2001).
93 This model also suggests that initiation of the rapid syntaxial exhumation could be
94 triggered by capture of the Yarlung Tsangpo by the Brahmaputra River (Zeitler et al., 2001).
95 However, both the timing of integration of the Yarlung Tsangpo-Brahmaputra River and
96 initiation of the rapid syntaxial exhumation continue to be debated (e.g. Bracciali et al.
97 2015, 2016; Najman et al., 2019).

98 It has been proposed that the Yarlung Tsangpo flowed southeastward into the
99 Irrawaddy River through the Parlung Tsangpo, before it was captured by the Siang-
100 Brahmaputra River at ~10 Ma (Brookfield, 1998) or 3–4 Ma (Zeitler et al., 2001; Clark et
101 al., 2004). The timing of this capture event was however estimated based on the proposed
102 age of the localized uplift of the eastern syntaxis. Recent provenance analyses of the paleo-
103 Brahmaputra deposits provide new time constraints on integration of the Yarlung Tsangpo-
104 Brahmaputra River, to be either in the Late Miocene or the Early Miocene. The first
105 appearance of Gangdese arc detritus, indicative of a Yarlung Tsangpo contribution, in the
106 eastern Himalayan foreland basin were detected at ~10 Ma (Cina et al., 2009), at ~7 Ma
107 (Chirouze et al., 2013) and in the Early Miocene (Lang and Huntington, 2014) in various
108 sections. Meanwhile, Bracciali et al. (2015) observed the first influx of Gangdese arc
109 material in Lower Miocene sediments of the Surma Basin (northeastern Bengal Basin)
110 downstream of the Brahmaputra River. The timing of onset of the rapid syntaxial
111 exhumation remains poorly constrained, varying from the Late Miocene to the Plio-

112 Pleistocene (11–2 Ma). Most of the bedrock thermochronology data from the syntaxial
113 region show young cooling ages and indicate onset of rapid exhumation since ~3.5 Ma (e.g.
114 [Burg et al., 1997](#); [Seward and Burg, 2008](#)). However, bedrock zircon U-Pb geochronology
115 denoted local melting accompanying rapid cooling since ~11–9.7 Ma ([Ding et al., 2001](#);
116 [Booth et al., 2004](#)). A synthesis study of cooling history within and around the syntaxis
117 indicates a significant pulse of rapid exhumation at 10–5 Ma ([Zeitler et al., 2014](#)). The
118 paleo-Brahmaputra detrital records could offer a long-term exhumation history of the
119 syntaxis after the integration of the Yarlung Tsangpo-Brahmaputra River, which avoids
120 problems associated with study of the syntaxis bedrock where erosion and metamorphism
121 have removed or obscured the early exhumation history. However, estimates of the onset
122 of rapid exhumation interpreted from detrital thermochronology are also variable. Rapid
123 exhumation was recorded in the eastern Himalayan foreland basin by 7–5 Ma ([Lang et al.,](#)
124 [2016](#)), in the Surma Basin since ~3.5–2 Ma ([Bracciali et al. 2016](#)) and in the Bengal Fan
125 since ~3.5 Ma ([Najman et al., 2019](#)), as indicated by the first occurrence of detrital minerals
126 with short lag times.

127 International Ocean Discovery Program (IODP) Expedition 362 successfully cored
128 Nicobar Fan sediments dating back to the Early Miocene (~19 Ma) ([Fig. 1](#)). These
129 sediments represent a key sedimentary archive of eastern Himalayan evolution ([McNeill](#)
130 [et al., 2017a, 2017b](#)). The Nicobar Fan sediments was transported for a long distance over
131 1700 km from the outlet. Therefore, compared to the proximal records of the fluvial-deltaic
132 Himalayan foreland basin and Surma Basin, the Nicobar Fan sediments might be expected
133 to minimize local effects that would obscure the upstream signal, and also provide a
134 continuous marine sedimentary succession with better depositional age constraints.

135 Evidence from the Bengal Basin and the Bay of Bengal indicates that the Ganges River
136 and the Brahmaputra River entered the Bay of Bengal separately at some time in the past
137 (e.g. [Curry et al. 2003](#); [Govin et al., 2018](#)), rather than merging together before entering
138 the bay as they do today. Therefore, compared to the Bengal Fan, the Nicobar Fan in the
139 east should be less influenced by the signal of the Ganges River that drains the central
140 Himalaya and peninsular India. Any significant contribution from the Irrawaddy River to
141 the Nicobar Fan is unlikely as it requires transfer of the sediments across the forearc to the
142 west, which was restricted by the then exposed Yadana-M8 Highs and the uplifted Sewell-
143 Alcock Rises west of the Andaman Sea ([Racey and Ridd, 2015](#)) ([Fig. 1](#)). Sediment
144 isopaches of the Cenozoic Martaban basin in the Andaman Sea related to the development
145 of the Salween-Irrawaddy delta also show no significant sediment transfer to the west
146 ([Racey and Ridd, 2015](#)) ([Fig. 1](#)). Because the Himalayan units and the Gangdese arc have
147 contrasting lithologies and geochemistry (e.g. [Singh et al., 2008](#); [Wu et al., 2010](#)) ([Table](#)
148 [1](#)), we conduct a provenance analysis of the Nicobar Fan sediments using trace elements
149 and Sr-Nd isotope composition. Specifically, we aim to constrain the timing of integration
150 of the Yarlung Tsangpo-Brahmaputra River by detecting the first appearance of Gangdese
151 arc material, and attempt to estimate the timing of initiation of rapid exhumation of the
152 eastern Himalayan syntaxis from the perspective of a provenance shift. Lastly, we evaluate
153 the interaction between the rapid syntaxial exhumation and the Yarlung Tsangpo-
154 Brahmaputra River evolution.

155

156 **2. Background**

157 *2.1. Tectonic setting of the eastern Himalaya*

158 The collision between the Indian and Eurasian plates, beginning at 65–43 Ma,
159 deformed and uplifted the northern margin of the Indian continent to form the Himalayan
160 orogen (Yin, 2006). The Himalaya is separated from the Lhasa block of the Eurasian plate
161 by the Indus-Yarlung Suture Zone (Fig. 1). The southern Lhasa block is intruded by
162 Cretaceous–Paleogene magmatic and volcanic rocks of the Andean-type Gangdese arc,
163 resulting from the northward subduction of the Tethyan Ocean (e.g. Copeland et al., 1995).
164 South of the suture, the Himalaya is classically divided into four lithotectonic units: the
165 Tethyan Himalaya (Paleoproterozoic–Eocene sedimentary cover), the Greater Himalaya
166 (medium- to high-grade Paleoproterozoic–Ordovician metamorphic crystalline rocks), the
167 Lesser Himalaya (Proterozoic–Cambrian metasedimentary and sedimentary rocks) and the
168 Sub-Himalaya (Cenozoic foreland basin sediments) (Yin, 2006) (Fig. 1). Rapid
169 exhumation of the Greater Himalaya at the rate of 2–5 mm/yr initiated at ~23 Ma,
170 associated with movement on the Main Central Thrust and the South Tibetan Detachment
171 System (Fig. 1), and ceased around 18–16 Ma in the western and central Himalaya and
172 around 14–10 Ma in the eastern Himalaya (Najman et al., 2019 and references therein).
173 The Gangdese arc shows significantly higher ϵ_{Nd} and lower $^{87}Sr/^{86}Sr$ than the Himalayan
174 units, while the Lesser Himalaya have the lowest ϵ_{Nd} and most radiogenic $^{87}Sr/^{86}Sr$ among
175 the Himalayan units (Singh et al., 2008; Wu et al., 2010) (Table 1).

176 The eastern Himalayan syntaxis is mainly composed of high-grade metamorphic
177 crystalline rocks of the Greater Himalaya, which forms the peak of Namche Barwa (7782
178 m) in the core of the syntaxis (Ding et al., 2001). The syntaxis is a north-plunging
179 antiformal and in part domal structure (Bracciali et al., 2016). The Greater Himalaya in the
180 syntaxis shared a similar tectonothermal history with that in the main belt of the Himalaya

181 before their evolution diverged in the Late Miocene (Najman et al., 2019). Thereafter, the
182 Greater Himalaya showed younger metamorphism and more rapid exhumation (up to 10
183 mm/yr or more) in the syntaxis. Along the sharply curved eastern Himalayan syntaxis, the
184 WNW-ESE trending Himalayan collisional belt passes abruptly into the N-S striking Indo-
185 Burman Ranges (Fig. 1). The Indo-Burman Ranges is divided laterally into two portions.
186 The Neogene Indo-Burman Ranges in the west represent Himalayan-derived Bengal-
187 Nicobar Fan sediments incorporated into the accretionary prism, whereas the Paleogene
188 Indo-Burman Ranges in the east were interpreted as forearc sediments equivalent to the
189 Central Myanmar Basin or trench sediments with significant input from the Burmese arc
190 (including the Wuntho-Popa Arc and the Cretaceous–Paleogene plutons intruding the
191 Mogok Metamorphic Belt) (Allen et al., 2008). The Burmese arc overall shows similar Sr-
192 Nd isotope compositions to the Gangdese arc (Wu et al., 2010; Lin et al., 2019) (Table 1).

193

194 *2.2.Litho-stratigraphy and age model of the Nicobar Fan*

195 The Nicobar Fan is separated from the Bengal Fan by the Ninetyeast Ridge (formed
196 from 77 to 43 Ma, Frey et al., 2015) and now being subducted beneath the Sumatra margin.
197 IODP Expedition 362 drilled two sites on the northern Nicobar Fan east of the Ninetyeast
198 Ridge in 2016, recovering the complete sedimentary succession at Site U1480 to a
199 basement depth of 1415.53 meter below seafloor (mbsf), and from 1149.7 mbsf to within
200 10s m of basement at 1500 mbsf at Site U1481 (McNeil et al., 2017a) (Figs. 1 and 2). At
201 Site U1480, Units I–IIIA (0–1310.02 mbsf) represent the Nicobar Fan and are composed
202 predominantly of siliciclastic sediment gravity-flow deposits (mostly turbidities) like the
203 Bengal Fan (McNeil et al., 2017a). Unit I is 26.42 m-thick, and contains calcareous mud

204 and interbeds of fine sand and mud. Unit II (1223.93 m-thick) is characterized by frequent
205 occurrence of fine sand and sandy silt alternating with mud and is divided into three
206 subunits. Unit IIIA is only 59.67 m-thick and contains gray-green and minor reddish-brown
207 mudstone with rare thin-bedded siltstone, representing the earliest depositional phase of
208 the fan. At Site U1481, the upper ~210 m of the sedimentary succession is equivalent to
209 Unit IIC at Site U1480, while the lower ~140 m corresponds to Unit IIIA but includes a
210 ~20 m-thick bed of fine-grained sandstone and siltstone at its base (McNeil et al., 2017a).

211 The shipboard age models of Expedition 362 sites were generated using microfossils
212 (McNeil et al., 2017a). Backman et al. (2019) later proposed a revised age model of Site
213 U1480 taking post-cruise biostratigraphic data into account. According to the above age
214 models, the base of the Nicobar Fan at Site U1480 (1250.35 mbsf) is estimated at ~15.3
215 Ma, however, the lowest Nicobar Fan sediments (1500 mbsf) at Site U1481 is estimated
216 older at ~19.2 Ma (Fig. 2). Thicker Unit IIIA at Site U1481 with older and coarser
217 siliciclastic sediments potentially reflects topographic variations, because the site is less
218 proximal to the Ninetyeast Ridge and has deeper basement. At both sites, sedimentation
219 rates increased dramatically and synchronously at ~9.2 Ma corresponding to the Units IIIA
220 and IIC boundary (Fig. 2), from 8–15 m/m.y. to ~220 m/m.y. (Fig. 5). This timing was
221 placed at ~9.5 Ma by McNeil et al. (2017b), but it should be ~9.2 Ma according to the age
222 models of McNeil (2017a) and Backman et al. (2019). At Site U1480, the high
223 sedimentation rate persisted, but decreased slightly to 65–125 m/m.y. at 5.9 Ma and
224 subsequently increased to 290 m/m.y. at ~2.4 Ma (Fig. 5). The sedimentation rate then
225 dropped to 3–42 m/m.y. since ~1.7 Ma (Units I and II boundary), which was interpreted as

226 fan abandonment due to tectonic blocking of the sediment routing to the Nicobar Fan by
227 the Ninetyeast Ridge as it collided with the Sunda margin (McNeil et al., 2017a).

228

229 **3. Methods**

230 We conducted trace element and Sr-Nd isotopic analyses on the bulk silicate fraction
231 of the Nicobar Fan muds/mudstones, in an attempt to trace provenance variations. A total
232 of sixty-eight core samples were collected (Fig. 2), primarily from the mud/mudstone of
233 the upper part of turbidite beds. The samples were leached with 2N acetic acid to remove
234 carbonates prior to element and isotopic analyses at the State Key Laboratory of Isotope
235 Geochemistry, Guangzhou Institute of Geochemistry, Chinese Academy of Sciences.
236 Trace elements of all the samples were measured on a Perkin-Elmer Sciex Elan 6000
237 inductively coupled plasma mass spectrometer (ICP-MS). Sr and Nd isotopic ratios of sixty
238 samples were analyzed on a MicroMass Isoprobe multicollector inductively coupled
239 plasma mass spectrometer (MC-ICP-MS). The $^{87}\text{Sr}/^{86}\text{Sr}$ ratios of thirteen samples could
240 not be measured because we failed to separate Sr from these samples. Analytical methods
241 are provided in full in [Supplementary Materials](#).

242

243 **4. Results**

244 Results of the trace element and Sr-Nd isotopic analyses of the silicate fraction of the
245 Nicobar Fan samples are listed in [Supplementary Tables A.1 and A.2](#), respectively.

246

247 *4.1.Trace elements*

248 The trace elements Rb, Th, Ta, Nb, Y, show higher concentrations in our samples
249 compared to the Upper Continental Crust (UCC) (Rudnick and Gao, 2003) (Fig. 3a).
250 Abundances of transitional elements, V, Sc, Co, Cr and Ni in the Nicobar Fan samples
251 are also higher than those of the UCC (Fig. 3a). Most samples share similar pattern of
252 trace elements, except that Co and Ni abundances show a considerably scatter and are
253 significantly higher in Unit IIIA than in Units I and II. In general, trace elements in the
254 Nicobar Fan samples show similar characteristics to those in the Himalayan-derived
255 Neogene Surma Basin and Bengal Fan sediments (Hossain et al., 2010; Crowley et al.,
256 1998), although Ta, Zr and Hf concentrations in the Surma Basin sediments are obviously
257 higher than those in the Nicobar Fan samples (Fig. 3a). Chondrite-normalized distribution
258 patterns of rare earth element (REE) concentrations in the Nicobar Fan samples are similar
259 to those of the UCC, as well as Neogene Surma Basin and Bengal Fan sediments, in
260 displaying light REEs enrichment, heavy REEs depletion and a negative Eu anomaly (Fig.
261 3b). Temporal variations of element contents and ratios however show an abrupt change
262 at ~9.2 Ma (boundary of Units II and IIIA) at both Sites U1480 and U1481, characterized
263 by marked rise in Th, Ta and Nb contents and La/Lu and La_N/Yb_N ratios but significant
264 drop in Cr/Th ratio (Fig. 4). Although highly variable in terms of these element contents
265 and ratios since ~9.2 Ma, the Unit II sediments overall show higher Th, Ta and Nb
266 contents, higher La/Lu and La_N/Yb_N ratios but lower Cr/Th ratio than those of the Unit
267 IIIA sediments.

268

269 *4.2.Sr and Nd isotopes*

270 The $^{87}\text{Sr}/^{86}\text{Sr}$ ratios of the Nicobar Fan samples vary from 0.719718 to 0.750453
271 (Table A.2). The Unit IIIA sediments show relatively uniform $^{87}\text{Sr}/^{86}\text{Sr}$ ratios ranging from
272 0.721300 to 0.731113 (average of 0.726131), which then increased rapidly and
273 concurrently by 0.03 units after ~9.2 Ma (the Units II and IIIA boundary) at both Sites
274 U1480 and U1481 (Fig. 5). Although highly variable between 0.723152 and 0.750453, the
275 $^{87}\text{Sr}/^{86}\text{Sr}$ ratios of the Unit II sediments (average of 0.734478) are generally higher than
276 those of the Unit IIIA sediments. However, the Unit I sediments have an average $^{87}\text{Sr}/^{86}\text{Sr}$
277 ratios of 0.722044, close to the Unit IIIA average.

278 The ϵ_{Nd} values range from -16.1 to -7.8 (Table A.2), and the temporal evolution is
279 negatively correlated with the $^{87}\text{Sr}/^{86}\text{Sr}$ ratios (Fig. 5). The Unit IIIA sediments have higher
280 ϵ_{Nd} values, ranging from -13.3 to -7.8 (average of -11.7), whereas the Unit II sediments
281 generally have lower ϵ_{Nd} values (average of -13.5) highly oscillating between -16.1 and -
282 10.5. An oscillatory decrease in ϵ_{Nd} values is observed around the Units II and IIIA
283 boundary (Fig. 5). The ϵ_{Nd} values decreased from -12.2 at 9.24 Ma to -14.7 at 8.76 Ma at
284 Site U1480, while it first increased from -11.9 at 9.26 Ma to -10.1 at 9.18 Ma but then
285 dropped to -14.8 at 8.72 Ma at Site U1481. The ϵ_{Nd} values of the Unit I samples are
286 concentrated in the range of -11.5 to -10.6 (average of -11.1).

287 The Nicobar Fan sediments overall exhibit negative correlations between ϵ_{Nd} versus
288 Th, Ta and Nb contents and La/Lu and $\text{La}_{\text{N}}/\text{Yb}_{\text{N}}$ ratios, and a positive correlation between
289 ϵ_{Nd} versus Cr/Th ratio (Fig. 6). Because Nd isotopes are not modified by mineral sorting
290 processes, we deduce that these trace element contents and ratios are not significantly
291 affected by mineral sorting but primarily controlled by the composition of the source areas
292 (the Himalaya and the Gangdese arc as discussed below).

293

294 **5. Discussion**

295 *5.1. Eastern Himalayan Provenance for the Nicobar Fan sediments*

296 The trace element and REE distribution patterns of the Nicobar Fan sediments denote
297 a Himalayan provenance dominated by sedimentary-metasedimentary rocks. However,
298 enrichment of the transitional elements relative to UCC indicates additional input of more
299 mafic rocks. The Nicobar Fan sediments also reflect mixing between felsic and
300 intermediate sources on a plot of Cr/Th versus Th/Sc (Fig. A.1). It is also noteworthy that
301 the Nicobar Fan sediments show higher ϵ_{Nd} values and lower $^{87}Sr/^{86}Sr$ ratios than
302 contemporary sediments in the Bengal Fan (France-Lanord et al., 1993; Galy et al., 1996;
303 Galy et al., 2010), the Nepalese foreland (Huyghe et al., 2001, 2005; Szulc et al., 2006),
304 and the eastern Himalayan foreland (Chirouze et al., 2013) through the Neogene (Fig. 5).
305 The fan sediments also have higher ϵ_{Nd} values and lower $^{87}Sr/^{86}Sr$ ratios than the Surma
306 Basin sediments in the Miocene (Bracciali et al., 2015) (Fig. 5). Here we employ a Sr-Nd
307 isotope diagram to distinguish the possible sources for the Nicobar Fan (Fig. 7a). To
308 understand the source-to-sink process from the Himalaya to the northeastern Indian Ocean,
309 we also compare Sr-Nd isotope compositions of the Nicobar Fan sediments with those of
310 modern sediments in the Ganges and Brahmaputra mainstreams upstream their confluence
311 in the Bengal delta (Singh and France-Lanord, 2002; Singh et al., 2008).

312 The Brahmaputra sediments have obviously higher ϵ_{Nd} values and lower $^{87}Sr/^{86}Sr$
313 ratios than the Ganges sediments (Table 1). They are separate from each other in the Sr-
314 Nd isotope diagram (Fig 7a). Such distinction reflects contributions from their drainage

315 basins. The Ganges River drains the central Tethyan, Greater and Lesser Himalayas as well
316 as peninsular India. Of these, the Greater and Lesser Himalayas make up most of the
317 sediment load of the Ganges River, with the Greater Himalaya contributing >65% of the
318 total (Singh et al., 2008). Sediment input from the Tethyan Himalaya lying in the rain
319 shadow and from peninsular India is estimated to be minor (Singh et al., 2008). The
320 Brahmaputra River drains the same units in the eastern Himalaya, with its upper reach, the
321 Yarlung Tsangpo, draining the Tethyan Himalaya and the Gangdese arc. Therefore, the
322 Brahmaputra River is characterized by significant input from the Gangdese arc, whereas
323 the Ganges River shows more input from the Lesser Himalaya (Fig 7a). The Sr-Nd isotope
324 compositions of the Nicobar Fan sediments are close to the field of the Brahmaputra
325 sediments with slightly higher ϵ_{Nd} values (Fig 7a), showing Greater Himalayan affinity
326 plus a significant Gangdese arc contribution, which could account for enrichment of the
327 transitional elements.

328 Although the Burmese arc has similar Sr-Nd isotope compositions to the Gangdese
329 arc (Table 1 and Fig 7a), it could not be the major contributor to the arc components in the
330 Nicobar Fan. Direct input from the Burmese arc to the Nicobar Fan is unlikely, because
331 the accretionary prism (the Paleogene Indo-Burman Ranges) was uplifted and emerged
332 around 39–37 Ma, as evidenced by the quasi-closed estuarine condition and the shift from
333 westward-directed deltaic system to southward-directed fluvial-deltaic system in the
334 forearc basin (the western Central Myanmar Basin) at that time (Licht et al., 2016; 2018).
335 The Paleogene Indo-Burman Ranges would thus have provided a barrier to transport of the
336 Burmese arc material westward. Therefore, during the Neogene, the Burmese arc material
337 would have been delivered by the Irrawaddy River flowing southward along the Central

338 Myanmar Basin and finally been trapped in the Martaban Basin ([Racey and Ridd, 2015](#)).
339 Although sediments from the arc-derived Paleogene Indo-Burman Ranges were regarded
340 as a significant contributor to the eastern Bay of Bengal in the last glacial-interglacial cycle
341 when the eastern Bengal Fan was inactive, they were speculated to be transported by ocean
342 surface currents driven by monsoon winds (e.g. [Colin et al., 1999](#); [Joussain et al., 2016](#)).
343 The Nicobar Fan was active during 19–1.7 Ma and dominated by sandy and muddy
344 turbidites ([Pickering et al., 2020](#)), which were primarily advected by turbidite currents
345 instead of surface currents. It is obvious that the small rivers draining the western flank of
346 the Indo-Burman Ranges could not supply turbidites to the distant Nicobar Fan sites.
347 Moreover, the anticyclonic/cyclonic surface circulation driven by summer/winter
348 monsoons in the Bay of Bengal are restricted north of 12°N (e.g. [Joussain et al., 2016](#)). We
349 thus do not expect that the Paleogene Indo-Burman Ranges material would reach the
350 Nicobar Fan sites near the Equator today and in the Southern Hemisphere during the
351 Miocene ([Hall, 2012](#)) ([Fig. 8](#)). Therefore, we exclude that the arc components in the
352 Nicobar Fan were recycled from the Paleogene Indo-Burman Ranges.

353 The Nicobar Fan sediments also overlap the range of Neogene sediments in the Surma
354 Basin which represent the paleo-Brahmaputra deposits ([Bracciali et al., 2015](#)). The close
355 affinity in Sr-Nd isotope compositions between the Nicobar Fan, the Surma Basin and the
356 Brahmaputra sediments implies that the Nicobar Fan sediments were primarily supplied by
357 the Brahmaputra River from the eastern Himalaya. Unlike the Nicobar Fan sediments, Sr-
358 Nd isotope compositions of the Bengal Fan sediments overlap both the ranges of the
359 Brahmaputra and the Ganges sediments ([Fig. 7a](#)), indicating a mixture of sediments derived
360 from the two rivers. The Nepalese foreland sediments have most affinity with the Ganges

361 sediments, displaying significant Lesser Himalaya input, as expected (Fig. 7a). Mixing of
362 the Ganges and Brahmaputra sediments in various proportions in the Bengal Fan during
363 the Neogene has also been demonstrated by detrital zircon U-Pb dating from Bengal Fan
364 IODP sites (Blum et al., 2018). In light of the temporal variation in detrital U-Pb age
365 populations, the Ganges River is known to have served as the major source of sediment to
366 the Bengal Fan prior to ~3.5 Ma, although it is nowadays mostly supplied by the
367 Brahmaputra River (Blum et al., 2018). The difference in Sr-Nd isotope compositions
368 between the Bengal Fan and the Nicobar Fan sediments implies that the Ganges and the
369 Brahmaputra Rivers used to deliver sediments separately to the Bay of Bengal through
370 independent river mouths and slope canyon-channel systems (Fig. 8). Mixing of Ganges
371 and Brahmaputra sediments by channel avulsions appears to have been common in the
372 Bengal Fan, but not in the Nicobar Fan, or the Nicobar Fan sediments would also plot
373 between the Ganges and the Brahmaputra sediments in the Sr-Nd isotope diagram.
374 Separation of the Ganges-Brahmaputra river mouths is evidenced by a paleo-Brahmaputra
375 course east of the Shillong Plateau, which was redirected west by the rising plateau and the
376 westward-propagated Indo-Burman Ranges at 5.2–4.9 Ma (Govin et al., 2018) (Figs. 8b
377 and 8c). However, it remains unknown when the two rivers first joined after then as river
378 avulsion might occurred frequently. Some clues indicate that the Ganges-Brahmaputra
379 River mouths were still separated at times during the Quaternary. For example, distribution
380 of the Bengal Fan sequences suggests two active canyon-channel systems during 1.9–0.96
381 Ma (Curray et al., 2003), which were probably fed by the Ganges River and Brahmaputra
382 River respectively. Therefore, compared to the Bengal Fan, the Nicobar Fan provides a
383 simpler erosion record of the eastern Himalaya that can be used to constrain the timing of

384 integration of the Yarlung Tsangpo-Brahmaputra River and initiation of the rapid syntaxial
385 exhumation.

386

387 *5.2. An integrated Yarlung Tsangpo-Brahmaputra River since Early Miocene*

388 The Sr-Nd isotope compositions of the Nicobar Fan sediments indicate an eastern
389 Himalayan source dominated by the Greater Himalaya but with significant Gangdese arc
390 contribution since ~19 Ma. It is noteworthy that the arc component in Unit IIIA is stronger
391 than that in Unit II, as indicated by the significantly higher Co and Ni contents (Fig. 3a),
392 lower Th, Ta and Nb contents, lower La/Lu and La_N/Yb_N ratios and higher Cr/Th ratios
393 (Fig. 4), as well as higher ϵ_{Nd} values and lower $^{87}Sr/^{86}Sr$ ratios (Figs. 5 and 7). The Unit
394 IIIA sediments also show higher ϵ_{Nd} values (-13.3 to -7.8) than modern Brahmaputra
395 sediments (-16.9 to -12.5) (Fig. 7a). Because Gangdese arc material in the Brahmaputra
396 River is presently strongly diluted by the Greater Himalayan detritus derived from the
397 rapidly exhuming eastern Himalayan syntaxis, the higher ϵ_{Nd} values seen in Unit IIIA
398 sediments at 19–9.2 Ma could reflect the Brahmaputra sedimentation prior to rapid
399 syntaxial exhumation. Determining the proportions of the Greater Himalaya and the
400 Gangdese arc contributing to the Nicobar Fan might be complex, because the Lesser and
401 Tethyan Himalayas would be part of the source mixture although their contributions are
402 minor. Nevertheless, we perform a simple two-components mixing model based on Sr-Nd
403 isotopes only regarding the Greater Himalaya and the Gangdese arc (Fig. 7b). In this model,
404 the proportion of the Gangdese arc material could be over ~50% in average in the Unit IIIA
405 sediments (Fig. 7b).

406 Airfall volcanic ash is occasionally found through Unit IIIA in form of very thin (0.5–
407 4 cm) ash layers (McNeill et al., 2017a), but we avoided collecting samples from these
408 layers. Except for a single sample (~16.7 Ma) with a high ϵ_{Nd} value (-7.8) (Fig. 5), the Unit
409 IIIA sediments show relatively stable $^{87}Sr/^{86}Sr$ ratios, ϵ_{Nd} values and element
410 concentrations and ratios at both Sites U1480 and U1481, indicating a long-term
411 continuous input from the Gangdese arc and no significant dispersed volcanic ash in the
412 samples. Moreover, the sample with a high ϵ_{Nd} value (-7.8) was collected from silty
413 mudstone within turbidite units, which obviously lack of volcanic ash. All the evidence
414 above suggests that igneous detritus instead of volcanic ash is responsible for the
415 geochemical characteristic of the Unit IIIA sediments.

416 The influence of Gangdese arc detritus in the Nicobar Fan is also supported by the
417 presence of typical Cretaceous–Eocene Gangdese zircons (Govin et al., 2018) throughout
418 the core samples, with the proportion of <150 Ma population ranging 2–17% (McNeil et
419 al., 2017b) (Fig. 5). The oldest sediments (~18 Ma) in Site U1451 on the Bengal Fan also
420 show 8% zircon grains of <150 Ma population (Blum et al., 2018). As the 75–50 Ma
421 population is absent in the Himalayan units and rare in the Bomi-Chayu batholith east of
422 the syntaxis, it can be regarded as an exclusive indicator of the Gangdese arc (Bracciali et
423 al., 2015; Lang and Huntington, 2014). This age population is found in the Nicobar Fan
424 sediments, particularly in the Lower Miocene sample, although only at <6% of the total
425 population (Fig. 5). Therefore, the detrital geochronology, along with our Sr-Nd isotope
426 results, show long-term continuous input from the Gangdese arc to the Nicobar Fan via the
427 Brahmaputra River. We thus propose an integrated Yarlung Tsangpo-Brahmaputra River
428 being active at least since the Early Miocene (~19 Ma) (Fig. 8a). This timing is compatible

429 with the results from the eastern Himalayan foreland near the Siang River (Lang and
430 Huntington, 2014) and from the Surma Basin (Bracciali et al., 2015), suggesting
431 connection of the Yarlung Tsangpo-Brahmaputra River through the Siang River.
432 Importantly, we provide improved age constraints because the depositional age of the
433 fluvial deposits is difficult to accurately determine. Our result also demonstrates the
434 diachronous arrival of Gangdese arc detritus in the eastern Himalayan foreland, which was
435 dated as ~10 Ma in the Subansiri River section (Cina et al., 2009), ~7 Ma in the Kameng
436 River section (Chirouze et al. 2013) and ~5 Ma farther west (Govin et al., 2018), arose
437 from the westward migration of the Brahmaputra course (Govin et al., 2018). However,
438 whether and when the Yarlung Tsangpo was captured by the Brahmaputra River remains
439 ambiguous. Bracciali et al. (2015) found no detrital zircons of Gangdese-age in two Upper
440 Eocene–Oligocene samples in the Surma Basin. Based on the sedimentary records in the
441 Central Myanmar Basin, Robinson et al. (2014) proposed that a Yarlung Tsangpo-
442 Irrawaddy River was established by 40 Ma and was then captured by the Brahmaputra
443 River before the Early Miocene. In contrast, Licht et al. (2016) found no evidence to
444 support a Yarlung Tsangpo-Irrawaddy connection. This might infer a long-lived Yarlung
445 Tsangpo-Brahmaputra River that was established before the Early Miocene, and it is
446 possible that the Brahmaputra River drained east of the Surma Basin at that time.

447

448 *5.3. Two-stage rapid exhumation of the eastern Himalayan syntaxis since Late Miocene*

449 The noteworthy increase in sedimentation rate at the Nicobar Fan sites at ~9.2 Ma was
450 interpreted as the result of the reduction in accommodation space of the Bengal Basin due
451 to the inversion of the Shillong Plateau and the westward encroachment of the Indo-Burma

452 Ranges, which increased sediment supply directly to the Nicobar Fan (McNeil et al.,
453 2017b). However, although the exhumation of the Shillong Plateau begun at 15–9 Ma
454 (Biswas et al., 2007), topographic growth of the plateau was chronologically decoupled
455 from the exhumation and did not initiate until 5.2–4.9 Ma (Govin et al., 2018) owing to the
456 contrasting erodibility between the sedimentary cover and the resistant basement rocks
457 (Biswas et al., 2007). The growth history of the Indo-Burma Ranges has not yet been
458 accurately dated. Thus, the sedimentation rate variation at ~9.2 Ma is hard to be interpreted
459 as a reflection of the reduction in continental accommodation space. Synchronous with the
460 acceleration in sedimentation rate, the abrupt change in trace element contents and ratios
461 and Sr-Nd isotope compositions around 9.2 Ma denotes a provenance shift (Figs. 4 and 5).
462 The decreasing ϵ_{Nd} values and increasing $^{87}Sr/^{86}Sr$ ratios implies increasing flux of Greater
463 and/or Lesser Himalayan material compared to Gangdese arc sediments (Fig. 7a). Although
464 the increase of Lesser Himalayan detritus in response to the Lesser Himalayan exhumation
465 was proposed in the western and central Himalayan forelands at 12–10 Ma (Huyghe et al.,
466 2001; Szulc et al., 2006), it has not yet been documented in the eastern Himalayan foreland.
467 The Lesser Himalaya could not be the primary source leading to the sediment geochemistry
468 and sedimentation rate changes of the Nicobar Fan at ~9.2 Ma. If that was the case then
469 post-9.2 Ma sediments would show extremely low ϵ_{Nd} values and high $^{87}Sr/^{86}Sr$ ratios like
470 the Nepalese foreland under such accelerating sedimentation rate (Fig. 7a).

471 Instead, we ascribe the changes in sediment geochemistry and sedimentation rate at
472 ~9.2 Ma to an increase in the flux of Greater Himalayan material (the proportion increased
473 from ~50% in Unit IIIA to ~70% in Unit II, Fig. 7b) linked to the rapid exhumation of the
474 Greater Himalayan crystalline rocks in the eastern Himalayan syntaxis (Fig. 8b). This

475 conclusion is also supported by the detrital apatite fission-track data from the Nicobar Fan;
476 apatite grains with short (<1 m.y. and even zero) lag times indicating rapid source-area
477 exhumation were observed at 9–2 Ma (Pickering et al., 2018). Initiation of rapid syntaxial
478 exhumation as reflected in the Nicobar Fan sediments (~9.2 Ma) is consistent with the older
479 onset ages, ~11–9.7 Ma (Ding et al., 2001; Booth et al., 2004) and ~10 Ma (Zeitler et al.,
480 2014), determined from the bedrock thermochronology and geochronology. It is also
481 compatible with the poorly dated constraints from detrital thermochronology from the
482 foreland sections downstream the Siang River, of 7–5 Ma or earlier (Lang et al., 2016).
483 Zeitler et al. (2014) proposed that rapid exhumation starting from ~10 Ma took place in a
484 broad syntaxial region including the easternmost Lhasa block (Fig. 8b). The variations of
485 the Sr-Nd isotope compositions and the sedimentation rate in Unit II suggest that the rapid
486 syntaxial exhumation was likely to have reduced around 6–5 Ma (Fig. 5), in agreement
487 with the model proposed by Zeitler et al. (2014).

488 An interval of very low ϵ_{Nd} values (-14 to -16) and high $^{87}\text{Sr}/^{86}\text{Sr}$ ratios (0.74 to 0.75)
489 in the Nicobar Fan sediment is observed again at 3.5–1.7 Ma when sedimentation rates
490 reached a peak of ~290 m/m.y. (Fig. 5) before Pleistocene fan abandonment. The
491 proportion of the Greater Himalayan material increase up to ~80% (Unit IIA average in
492 Fig. 7b). This episode is coeval with the previously proposed younger onset age of the
493 syntaxial exhumation at ~3.5 Ma based on most of the bedrock thermochronology data (e.g.
494 Burg et al., 1997; Seward and Burg, 2008). This younger pulse of rapid exhumation since
495 ~3.5 Ma was stronger but only focused in the Namche Barwa massif, defined as the core
496 of the syntaxis northeast of the Nam La Thrust (Zeitler et al., 2014) (Fig. 8c). It is also
497 witnessed in the Bengal Fan and the Surma Basin, as evidenced by the presence of detrital

498 minerals with <1 m.y. lag times since ~3.5 Ma (Najman et al., 2019; Bracciali et al. 2016).
499 The absence of this signal of rapid syntaxial exhumation in the Bengal Fan between 9.2
500 and 3.5 Ma might be due to strong supply of the Ganges sediments to that depocenter (Blum
501 et al., 2018). The variations in sediment geochemistry and sedimentation rate seen at ~9.2
502 Ma in the Nicobar Fan were not observed in the Bengal Fan sites either. The stronger
503 exhumation pulse since ~3.5 Ma enabled more Brahmaputra sediments to be delivered into
504 the Bengal Fan (Fig. 8c), as indicated by the increase of Gangdese-age zircons and the first
505 appearance of short-lag time minerals (Blum et al., 2018; Najman et al., 2019). However,
506 it is puzzling that the signal of rapid syntaxial exhumation did not appear until 3.5–2.0 Ma
507 in the Surma Basin, at odds with the presence of Gangdese arc material since the Early
508 Miocene (Bracciali et al., 2015, 2016). This mis-match might result from the effects of
509 dilution, hydraulic sorting and grain size.

510 The sedimentary record from the Nicobar Fan favors a two-stage exhumation model
511 of the eastern Himalayan syntaxis. Despite the sedimentation rate and provenance
512 variations, more specific detrital thermochronological work needs to be done on the
513 Nicobar Fan to test this model. Regardless of whether the rapid syntaxial exhumation
514 initiated at ~9.2 Ma or ~3.5 Ma these times significantly postdated the integration of the
515 Yarlung Tsangpo-Brahmaputra River before ~19 Ma. If the capture of the Yarlung
516 Tsangpo by the Brahmaputra River occurred it would be at least 10 m.y. older than the
517 inception of rapid exhumation. Therefore, drainage capture followed by focused incision
518 cannot be responsible for the initiation of the rapid syntaxial exhumation as proposed by
519 the tectonic aneurysm model (Zeitler et al., 2001). Instead, the rapid exhumation must have
520 been initiated by tectonic uplift driven by the northward indentation of the northeastern

521 corner of the Indian Plate (e.g. [Burg et al., 1997](#); [Seward and Burg, 2008](#); [Bendick and](#)
522 [Ehlers, 2014](#)), which also distorted the course of the antecedent Yarlung Tsangpo-
523 Brahmaputra River. The rock uplift, probably coupled with monsoon precipitation, would
524 have enhanced river incision. A positive feedback between tectonics and erosion would
525 thus have been established. Therefore, we do not exclude the tectonic aneurysm model
526 ([Zeitler et al., 2001; 2004](#)) as the primary mechanism for sustaining or accelerating rapid
527 syntaxial exhumation.

528

529 **6. Conclusions**

530 We conducted a provenance study on well-dated Nicobar Fan sediments (19 Ma–
531 Recent) using trace element and Sr-Nd isotopic methods. We provide new time constraints
532 for integration of the Yarlung Tsangpo-Brahmaputra River and initiation of rapid
533 exhumation of the eastern Himalayan syntaxis.

534 The trace element and REE distribution patterns of the Nicobar Fan sediments indicate
535 a Himalayan provenance. The Sr-Nd isotope compositions of the Nicobar Fan sediments
536 further show a close affinity with Brahmaputra sediments dominated by the Greater
537 Himalayan material but also with significant contributions from the Gangdese arc,
538 demonstrating that the Nicobar Fan sediments were primarily supplied by the Brahmaputra
539 River from the eastern Himalaya. The geochemical and Sr-Nd isotope compositions of the
540 lower part of the Nicobar Fan indicate long-term continuous input of Gangdese arc material
541 to the deep sea, and therefore imply an integrated Yarlung Tsangpo-Brahmaputra River
542 flowing at least since the Early Miocene (~19 Ma). Based on variations in sedimentation

543 rate and provenance of the Nicobar Fan, we favor a two-stage rapid exhumation model of
544 the eastern Himalayan syntaxis. The abrupt change in geochemical and isotope
545 compositions synchronous with the acceleration in sedimentation rate at ~9.2 Ma indicates
546 increasing flux of Greater Himalaya material in response to the rapid exhumation
547 commencing across a wide region of the eastern Himalayan syntaxis. The very low ϵ_{Nd}
548 values and high $^{87}Sr/^{86}Sr$ ratios at 3.5–1.7 Ma, accompanying the peak sedimentation rate,
549 corresponds to a younger pulse of rapid exhumation focused in the core of the syntaxis
550 since ~3.5 Ma. Because initiation of rapid syntaxial exhumation postdated the integration
551 of the Yarlung Tsangpo-Brahmaputra River by at least 10 m.y., this must have been
552 triggered by tectonic uplift instead of capture of the Yarlung Tsangpo by the Brahmaputra
553 River. A positive feedback between tectonics and erosion would have been established
554 subsequently.

555

556 **Acknowledgements**

557 This research used samples and data provided by the International Ocean Discovery
558 Program (IODP). We appreciate Science Party of IODP Expedition 362, in particular the
559 Co-Chief Scientists (McNeill L.C. and Dugan B.E.) and the Staff Scientist (Petronotis
560 K.E.), for their efforts. We also thank the IODP staff and JOIDES Resolution crew for their
561 contributions during the expedition. This research was financially supported by the
562 National Natural Science Foundation of China (grant 41606068), research grants from the
563 Key Special Project for Introduced Talents of Southern Marine Science and Engineering
564 Guangdong Laboratory (Guangzhou) (GML2019ZD0202), the National Programme on
565 Global Change and Air-Sea Interaction (GASI-GEOGE-02), and Innovation Academy of

566 South China Sea Ecology and Environmental Engineering, Chinese Academy of Sciences
567 (ISEE2020YB07), and the Research Fund Program of Guangdong Provincial Key
568 Laboratory of Marine Resources and Coastal Engineering (grant GDKLMRCE1804). This
569 is contribution IS-XXXX from GIGCAS. We thank Sun Shengling and Zhang Le for their
570 help on the analyses in GIGCAS laboratories and thank Kutterolf Steffen for his helpful
571 discussion. We are grateful to the editor and two anonymous reviewers for their valuable
572 comments which have substantially improved the paper. All the data used in this paper are
573 provided in Supplementary materials.

574

575 **References**

- 576 Allen, R., Najman, Y., Carter, A., Parrish, R., Bickle, M., Paul, M., Garzanti, E., Reisberg,
577 L., Chapman, H., Vezzoli, G., Andò, S., 2008. Provenance of the Tertiary sedimentary
578 rocks of the Indo-Burman Ranges, Burma (Myanmar): Burman arc or Himalayan-
579 derived? *J. Geol. Soc. London* 165, 1045–1057. [https://doi.org/10.1144/0016-](https://doi.org/10.1144/0016-76492007-143)
580 [76492007-143](https://doi.org/10.1144/0016-76492007-143).
- 581 Backman, J., Chen, W., Kachovich, S., Mitchison, F., Petronotis, K., Yang, T., Zhao, X.,
582 2019. Data report: revised age models for IODP Sites U1480 and U1481, Expedition
583 362, in: McNeill, L.C., Dugan, B., Petronotis, K.E., the Expedition 362
584 Scientists, Sumatra Subduction Zone. *Proc. IODP*, vol. 362. International Ocean
585 Discovery Program, College Station, TX.
586 <https://doi.org/10.14379/iodp.proc.362.202.2019>.
- 587 Bendick, R., Ehlers, T.A., 2014. Extreme localized exhumation at syntaxes initiated by

588 subduction geometry. *Geophys. Res. Lett.* 41(16), 5861–5867.

589 Biswas, S., Coutand, I., Grujic, D., Hager, C., Stöckli, D., Grasemann, B., 2007.

590 Exhumation and uplift of the Shillong plateau and its influence on the eastern

591 Himalayas: New constraints from apatite and zircon (U-Th-[Sm])/He and apatite

592 fission track analyses. *Tectonics* 26, TC6013.

593 Blum, M., Rogers, K., Gleason, J., Najman, Y., Cruz, J., Fox, L., 2018. Allogenic and

594 autogenic signals in the stratigraphic record of the deep-sea Bengal Fan. *Sci. Rep.* 8,

595 7973.

596 Booth, A.L., Zeitler, P.K., Kidd, W.S.F., Wooden, J., Liu, Y.P., Idleman, B., Hren, M.,

597 Chamberlain, C.P., 2004. U-Pb zircon constraints on the tectonic evolution of

598 southeastern Tibet, Namche Barwa area. *Am. J. Sci.* 304, 889–929.

599 Bracciali, L., Najman, Y., Parrish, R.R., Akhter, S.H., Millar, I., 2015. The Brahmaputra

600 tale of tectonics and erosion: Early Miocene river capture in the eastern Himalaya.

601 *Earth Planet. Sci. Lett.* 415, 25–37.

602 Bracciali, L., Parrish, R.R., Najman, Y., Smye, A., Carter, A., Wijbrans, J.R., 2016. Plio-

603 Pleistocene exhumation of the eastern Himalayan syntaxis and its domal ‘pop-up’.

604 *Earth-Sci. Rev.* 160, 350–385.

605 Brookfield, M.E., 1998. The evolution of the great river systems of southern Asia during

606 the Cenozoic India-Asia collision: Rivers draining southwards. *Geomorphology* 22,

607 285–312.

608 Burg, J.P., Davy, P., Nievergelt, P., Oberli, F., Seward, D., Diao, Z., Meier, M., 1997.

609 Exhumation during crustal folding in the Namche-Barwa syntaxis. *Terra Nova* 9, 53–

610 56.

611 Chirouze, F., Huyghe, P., van der Beek, P., Chauvel, C., Chakraborty, T., Dupont-Nivet, G.,
612 Bernet, M., 2013. Tectonics, exhumation, and drainage evolution of the eastern
613 Himalaya since 13 Ma from detrital geochemistry and thermochronology, Kameng
614 River Section, Arunachal Pradesh. *Geol. Soc. Am. Bull.* 125(3–4), 523–538.

615 Cina, S.E., Yin, A., Grove, M., Dubey, C.S., Shukla, D.P., Lovera, O.M., Kelty T.K.,
616 Gehrels G.E., Foster D.A., 2009. Gangdese arc detritus within the eastern Himalayan
617 Neogene foreland basin: Implications for the Neogene evolution of the Yalu-
618 Brahmaputra river system. *Earth Planet. Sci. Lett.* 285(1–2), 0–162.

619 Clark, M.K., Schoenbohm, L.M., Royden, L.H., Whipple, K.X., Burchfiel, B.C., Zhang,
620 X., Tang, W., Wang, E., Chen, L., 2004. Surface uplift, tectonics, and erosion of
621 eastern Tibet from large-scale drainage patterns. *Tectonics* 23(1), TC1006.

622 Colin, C., Turpin, L., Bertaux, J., Desprairies, A., Kissel, C., 1999. Erosional history of the
623 Himalayan and Burman ranges during the last two glacial–interglacial cycles. *Earth
624 Planet. Sci. Lett.* 171(4), 647–660.

625 Copeland, P., Harrison, T.M., Pan, Y., Kidd, W., Roden, M., Zhang, Y., 1995. Thermal
626 evolution of the Gangdese batholith, southern Tibet: a history of episodic un-roofing.
627 *Tectonics* 14, 223–236.

628 Crowley, S.F., Stow, D.A.V., Croudace, I.W., 1998. Mineralogy and geochemistry of Bay
629 of Bengal deep-sea fan sediments, ODP Leg 116: evidence for an Indian subcontinent
630 contribution to distal fan sedimentation, in: Cramp, A., MacLeod, C.J., Lee, S.V.,
631 Jones, E.J.W. (Eds.), *Geological Evolution of Ocean Basins: Results from the Ocean
632 Drilling Program*. *Geol. Soc. London Spec. Publ.* 131, 151–176.

633 Curray, J.R., Emmel, F.J., Moore, D.G., 2003. The Bengal Fan: morphology, geometry,

634 stratigraphy, history and processes. *Mar. Petrol. Geol.* 19(10), 1191–1223.

635 Ding, L., Zhong, D., Yin, A., Kapp, P., Harrison, T.M., 2001. Cenozoic structural and
636 metamorphic evolution of the eastern Himalayan syntaxis (Namche Barwa). *Earth*
637 *Planet. Sci. Lett.* 192, 423–438.

638 France-Lanord, C., Derry, L., Michard, A., 1993. Evolution of the Himalaya since Miocene
639 time: isotopic and sedimentological evidence from the Bengal Fan. *Geol. Soc. London*
640 *Spec. Publ.* 74(1), 603–621.

641 Frey, F.A., Silva, I.G.N., Huang, S., Pringle, M.S., Meleney, P.R., Weis, D. 2015. Depleted
642 components in the source of hotspot magmas: Evidence from the Ninetyeast Ridge
643 (Kerguelen). *Earth and Planetary Science Letters*, 426, 293-304.

644 Galy, A., France-Lanord, C., Derry, L.A., 1996. The Late Oligocene-Early Miocene
645 Himalayan belt constraints deduced from isotopic compositions of Early Miocene
646 turbidites in the Bengal Fan. *Tectonophysics* 260(1–3), 109–118.

647 Galy, V., France-Lanord, C., Peucker-Ehrenbrink, B., Huyghe, P., 2010. Sr-Nd-Os evidence
648 for a stable erosion regime in the Himalaya during the past 12 Myr. *Earth Planet. Sci.*
649 *Lett.* 290(3–4): 0–480.

650 Govin, G., Najman, Y., Copley, A., Millar, I., van der Beek, P., Huyghe, P., Grujic D.,
651 Davenport J., 2018. Timing and mechanism of the rise of the Shillong Plateau in the
652 Himalayan foreland. *Geology* 46 (3), 279–282. doi: <https://doi.org/10.1130/G39864.1>

653 Hall, R., 2012. Late Jurassic–Cenozoic reconstructions of the Indonesian region and the
654 Indian Ocean. *Tectonophysics* 570–571, 1–41.
655 <http://dx.doi.org/10.1016/j.tecto.2012.04.021>.

656 Hossain, H.M.Z., Roser, B.P., Kimura, J.I., 2010. Petrography and whole-rock

657 geochemistry of the Tertiary Sylhet succession, northeastern Bengal Basin,
658 Bangladesh: Provenance and source area weathering. *Sediment. Geol.* 228(3–4), 171–
659 183.

660 Huyghe, P., Galy, A., Mugnier, J. L., France-Lanord, C., 2001. Propagation of the thrust
661 system and erosion in the Lesser Himalaya: Geochemical and sedimentological
662 evidence. *Geology* 29(11), 1007–1010.

663 Huyghe, P., Mugnier, J.L., Gajurel, A.P., Delcaillau, B., 2005. Tectonic and climatic control
664 of the changes in the sedimentary record of the Karnali River section (Siwaliks of
665 western Nepal). *Island Arc* 14(4), 311–327.

666 Jousain, R., Colin, C., Liu, Z., Meynadier, L., Fournier, L., Fauquembergue, K., Zaragosi,
667 S., Schmidt, F., Rojas, V., Bassinot, F., 2016. Climatic control of sediment transport
668 from the Himalayas to the proximal NE Bengal Fan during the last glacial-interglacial
669 cycle. *Quaternary Sci. Rev.* 148, 1–16.

670 Lang, K.A., Huntington, K.W., 2014. Antecedence of the Yarlung-Siang-Brahmaputra
671 River, eastern Himalaya. *Earth Planet. Sci. Lett.* 397, 145–158.

672 Lang, K.A., Huntington, K.W., Burmester, R., Housen, B., 2016. Rapid exhumation of the
673 eastern Himalayan syntaxis since the late Miocene. *Geol. Soc. Am. Bull.* 128(9),
674 1403–1422.

675 Licht, A., Reisberg, L., France-Lanord, C., Soe, A.N., Jaeger, J.J., 2016. Cenozoic
676 evolution of the Central Myanmar drainage system: insights from sediment
677 provenance in the Minbu Sub-Basin. *Basin Res.* 28(2), 237–251.

678 Licht, A., Dupont-Nivet, G., Win, Z., Swe, H.H., Kaythi, M., Roperch, P., Ugrai, T., Littell,
679 V., Park, D., Westerweel, J., Jones, D., Poblete, F., Aung, D.W., Huang, H., Hoorn, C.,

680 Sein, K., 2018. Paleogene evolution of the Burmese forearc basin and implications for
681 the history of India-Asia convergence. *Geol. Soc. Am. Bull.* 131 (5-6), 730–748.
682 <https://doi.org/10.1130/B35002.1>.

683 Lin, T.H., Mitchell, A.H., Chung, S.L., Tan, X.B., Tang, J.T., Oo, T., Wu, F.Y., 2019. Two
684 parallel magmatic belts with contrasting isotopic characteristics from southern Tibet
685 to Myanmar: zircon U–Pb and Hf isotopic constraints. *J. Geol. Soc.* 176(3), 574–587.

686 McNeill, L.C., Dugan, B., Petronotis, K.E., the Expedition 362 Scientists, 2017a. Sumatra
687 Subduction Zone. *Proc. IODP*, vol. 362. International Ocean Discovery Program,
688 College Station, TX.

689 McNeill, L.C., Dugan, B., Backman, J., Pickering, K.T., Poudroux, H.F.A., Henstock, T.J.,
690 Petronotis, K.E., Carter, A., Chemale Jr., F., Milliken, K.L., Kutterolf, S., Mukoyoshi,
691 H., Chen, W., Kachovich, S., Mitchison, F.L., Bourlange, S., Colson, T.A., Frederik,
692 M.C.G., Guèrin, G., Hamahashi, M., House, B.M., Hüpers, A., Jeppson, T.N.,
693 Kenigsberg, A.R., Kuranaga, M., Nair, N., Owari, S., Shan, Y., Song, I., Torres, M.E.,
694 Vannucchi, P., Vrolijk, P.J., Yang, T., Zhao, X., and Thomas, E., 2017b. Understanding
695 Himalayan erosion and the significance of the Nicobar Fan. *Earth Planet. Sci. Lett.*
696 475, 134–142.

697 Najman, Y., Mark, C., Barfod, D. N., Carter, A., Parrish, R., Chew, D., Gemignani, L. 2019.
698 Spatial and temporal trends in exhumation of the Eastern Himalaya and syntaxis as
699 determined from a multitechnique detrital thermochronological study of the Bengal
700 Fan. *Geol. Soc. Am. Bull.* 131 (9–10), 1607–1622. <https://doi.org/10.1130/B35031.1>

701 Pickering, K.T., Poudroux, H., Carter, A., Andò, S., Garzanti, E., Limonta, M., Vezzoli,
702 G., Milliken, K.L., Chemale Jr., F., Mukoyoshi, H., Kutterolf, S. 2018. Sediment

703 Provenance and Depositional History of the Nicobar Fan (Bengal Depositional
704 System) from IODP Expedition 362: Detrital Zircon Geochronology, Apatite
705 Thermochronometry, Sand Petrography and Heavy-Mineral Results. In AGU Fall
706 Meeting Abstracts.

707 Pickering, K.T., Pouderoux, H., McNeill, L.C., Backman, J., Chemale, F., Kutterolf, S.,
708 Milliken, K.L., Mukoyoshi, H., Henstock, Timothy, J., Stevens, D.E., Parnell, C.,
709 Dugan, B., 2020. Sedimentology, stratigraphy and architecture of the Nicobar Fan
710 (Bengal–Nicobar Fan System), Indian Ocean: Results from International Ocean
711 Discovery Program Expedition 362. *Sedimentology*. doi: 10.1111/sed.12701.

712 Racey, A., Ridd, M.F., 2015. Petroleum geology of the Moattama region, Myanmar, in:
713 Racey, A., Ridd, M.F. (Eds.), *Petroleum geology of Myanmar*. Geol. Soc. Lond. Mem.
714 45, pp. 63–81.

715 Robinson, R.A.J., Brezina, C.A., Parrish, R.R., Horstwood, M.S.A., Oo, N.W., Bird, M.I.,
716 Thein, M., Walters, A.S., Oliver, G.J.H., Zaw, K., 2014. Large rivers and orogens: The
717 evolution of the Yarlung Tsangpo-Irrawaddy system and the eastern Himalayan
718 syntaxis. *Gondwana Res.* 26(1), 112–121.

719 Rudnick, R.L., Gao, S., 2003. Composition of the continental crust, in: Rudnick, R.L. (Ed.),
720 *Treatise on Geochemistry*, vol. 3, The Crust. Elsevier, New York, pp. 1–64.

721 Seward, D., Burg, J. P., 2008. Growth of the Namche Barwa Syntaxis and associated
722 evolution of the Tsangpo Gorge: constraints from structural and thermochronological
723 data. *Tectonophysics* 451, 282–289.

724 Singh, S.K., France-Lanord, C., 2002. Tracing the distribution of erosion in the
725 Brahmaputra watershed from isotopic compositions of stream sediments. *Earth Planet.*

726 Sci. Lett. 202(3), 645–662.

727 Singh, S.K., Rai, S.K., Krishnaswami, S., 2008. Sr and Nd isotopes in river sediments from
728 the Ganga Basin: Sediment provenance and spatial variability in physical erosion. *J.*
729 *Geophys. Res. Earth Surface*, 113: F03006.

730 Sun, S.S., McDonough, W.S., 1989. Chemical and isotopic systematics of oceanic basalts:
731 Implications for mantle composition and processes. *Geol. Soc. London, Spec. Publ.*
732 42(1), 313–345. <https://doi.org/10.1144/GSL.SP.1989.042.01.19>

733 Szulc, A.G., Najman, Y., Sinclair, H.D., Pringle, M., Bickle, M., Chapman, H., Garzanti E.,
734 Andò, DeCelles, P., 2006. Tectonic evolution of the Himalaya constrained by detrital
735 ^{40}Ar - ^{39}Ar , Sm-Nd and petrographic data from the Siwalik foreland basin succession,
736 SW Nepal. *Basin Res.* 18(4), 375–391.

737 Wu, W., Xu, S., Yang, J., Yin, H., Lu, H., Zhang, K., 2010. Isotopic characteristics of river
738 sediments on the Tibetan Plateau. *Chem. Geol.* 269(3–4), 406–413.

739 Yin, A., 2006. Cenozoic tectonic evolution of the Himalayan orogen as constrained by
740 along-strike variation of structural geometry, exhumation history, and foreland
741 sedimentation. *Earth-Sci. Rev.* 76(1–2), 1–131.

742 Zeitler, P.K., Meltzer, A.S., Koons, P.O., Craw, D., Hallet, B., Chamberlain, C.P., Kidd,
743 W.S.F., Park, S.K., Seeber, L., Bishop, M., Shroder, J., 2001. Erosion, Himalayan
744 geodynamics, and the geomorphology of metamorphism. *GSA Today* 11: 4–8.

745 Zeitler, P.K., Meltzer, A.S., Brown, L., Kidd, W.S.F., Lim, C., Enkelmann, E., 2014.
746 Tectonics and topographic evolution of Namche Barwa and the easternmost Lhasa
747 Block, in: Nie, J., Hoke, G.D., Horton, B. (Eds.), *Towards an Improved Understanding*
748 *of Uplift Mechanisms and the Elevation History of the Tibetan Plateau. Spec. Pap.,*

750

751 **Figure Captions (color online only for all figures)**

752 **Fig. 1.** Regional map of the Bengal-Nicobar Fan system, showing the IODP Expedition
753 362 sites (U1480 and U1481) on the Nicobar Fan and the relevant drilling sites of DSDP
754 Leg 22 (Site 218), ODP Leg 116 (Sites 717 and 718) and IODP Expedition 354 (Sites
755 U1449–U1455). The superimposed simplified geological map of the eastern Himalaya,
756 southeastern Tibet and Myanmar region, showing major terrains, terrain boundaries,
757 geological units and modern major rivers, is modified from [Robinson et al. \(2014\)](#) and
758 [Licht et al. \(2016\)](#). The Bengal Fan and the Nicobar Fan are outlined in black and grey,
759 respectively (after [Pickering et al., 2020](#)). The Martaban basin in the eastern Andaman Sea
760 is delineated by 3 km isopach ([Racey and Ridd, 2015](#)) in purple.

761

762 **Fig. 2.** Schematic lithological columns of Sites U1480 and U1481 modified from [McNeill](#)
763 [et al. \(2017a\)](#), showing the position of the Nicobar Fan samples.

764

765 **Fig. 3.** (a) Upper continental crust (UCC) ([Rudnick and Gao, 2003](#)) normalized for trace
766 elements in the Nicobar Fan samples, as compared with the Neogene sediments of the
767 Surma Basin ([Hossain et al., 2010](#)) and the Bengal Fan ([Crowley et al., 1998](#)). (b)
768 Chondrite-normalized REE distribution plot for the Nicobar Fan samples as compared with
769 the UCC and the Neogene sediments of the Surma Basin ([Hossain et al., 2010](#)) and the
770 Bengal Fan ([Crowley et al., 1998](#)). The chondrite values are cited from [Sun and](#)
771 [McDonough \(1989\)](#).

772

773 **Fig. 4.** Downhole variation of Th, Ta and Nb concentrations, and Cr/Th, La/Lu and
774 La_N/Yb_N ratios of the Nicobar Fan sediments at both Sites U1480 and U1481. Age of the
775 Site U1480 and U1481 samples is converted from the mid-point depth according to age
776 models of [Backman et al. \(2019\)](#) and [McNeil et al \(2017a\)](#), respectively.

777

778 **Fig. 5.** Downhole variation of Sr-Nd isotopic compositions of the Nicobar Fan sediments
779 at both Sites U1480 and U1481, as compared with the Sr-Nd isotopic compositions of
780 contemporary sediments in the Bengal Fan ([France-Lanord et al., 1993](#); [Galy et al., 1996](#);
781 [Galy et al., 2010](#)), the Surma Basin ([Bracciali et al., 2015](#)), the eastern Himalayan foreland
782 ([Chirouze et al., 2013](#)) and the Nepalese foreland ([Huyghe et al., 2001, 2005](#); [Szulc et al.,](#)
783 [2006](#)) and modern sediments in the Brahmaputra and the Ganges mainstreams ([Singh and](#)
784 [France-Lanord, 2002](#); [Singh et al., 2008](#)). All the ϵ_{Nd} values and $^{87}Sr/^{86}Sr$ ratios are
785 recalculated at time $T=0$, and depositional ages of the Surma Basin samples are of large
786 uncertainties. Also shown are the sedimentation rate of Sites U1480 and U1481 ([McNeill](#)
787 [et al., 2017a](#), [Backman et al., 2019](#)), ODP Site 718C (after [McNeill et al., 2017b](#)) and DSDP
788 Site 218 ([Galy et al., 2010](#)), the proportion of detrital zircons <150 Ma of the Nicobar Fan
789 samples ([McNeill et al. 2017b](#)), and the associated Himalayan tectonic events. GR=Ganges
790 River, BR=Brahmaputra River, NER=Ninetyeast Ridge.

791

792 **Fig. 6.** ϵ_{Nd} vs Th, Ta, Nb contents and Cr/Th, La/Lu and La_N/Yb_N ratios for the Nicobar
793 Fan samples. The grey dash lines in the plots represent the regression lines.

794

795 **Fig. 7.** (a) ϵ_{Nd} vs $^{87}\text{Sr}/^{86}\text{Sr}$ plot of the Nicobar Fan samples, as compared with the potential
796 source rocks from the Himalaya-Tibet region and the modern sediments in the Brahmaputra
797 and the Ganges mainstreams (see Table 1 for references). The composition fields of the
798 Neogene sediments in the Bengal Fan, the Surma Basin and the Nepalese foreland are also
799 shown (France-Lanord et al., 1993; Galy et al., 1996; Galy et al., 2000; Bracciali et al.,
800 2015; Huyghe et al., 2001; 2005). (b) A simple two-components mixing model based on
801 Sr-Nd isotopes for the Nicobar Fan sediments. End-member compositions used in the
802 model are: the Greater Himalaya: Sr=70 ppm, Nd=45 ppm, $^{87}\text{Sr}/^{86}\text{Sr}=0.760$, $\epsilon_{\text{Nd}}=-16$ (Singh
803 and France-Lanord, 2002; Singh et al., 2008); the Gangdese arc: Sr=200 ppm, Nd=34 ppm;
804 $^{87}\text{Sr}/^{86}\text{Sr}=0.715$; $\epsilon_{\text{Nd}}=-6.8$ (Wu et al., 2010). The latter is based on the average of the modern
805 river sediments from the tributaries and mainstream of the Yarlung Tsangpo that drain the
806 southern Lhasa block. It should be noted that in this calculation the proportion of the
807 Gangdese arc also includes the Pre-Cambrian basement rocks (the Nyainqêntanglha Group)
808 and the Paleozoic–Mesozoic sedimentary cover of the Lhasa block and even the Northern
809 Magmatic belt intruded the northern Lhasa block, besides the Cretaceous–Paleogene
810 magmatic and volcanic rocks (the Gangdese batholith and Linzizong volcanics) in the
811 southern Lhasa block, because the tributaries of the Yarlung Tsangpo also drain these units.
812 This might be one of the reasons why the proportion of Gangdese arc material derived from
813 this model is much higher than the proportion of typical Gangdese zircons (<150 Ma) in
814 the Nicobar Fan sand/sandstone (McNeil et al., 2017b) in Fig. 5 (other reasons might
815 include the abundance of zircons in parent rocks and hydraulic sorting of detrital zircons
816 during transport).

817

818 **Fig. 8.** Paleogeography reconstruction of the region of the northeastern Indian Ocean
 819 (adapted from [Hall, 2012](#)), showing drainage evolution of the Ganges River and the
 820 Yarlung Tsangpo-Brahmaputra River (modified from [Lang and Huntington, 2014](#); [Govin](#)
 821 [et al., 2018](#)) and the source-to-sink process from the Himalaya to the Bengal-Nicobar Fan
 822 system. GR=Ganges River, BR=Brahmaputra River, IR=Irrawaddy River, SP=Shillong
 823 Plateau, IBR=Indo-Burman Ranges, WPA=Wuntho-Popa Arc (Burmese arc),
 824 NER=Ninetyeast Ridge.

825

826 **Tables**

827 Table 1. $^{87}\text{Sr}/^{86}\text{Sr}$ ratios and ϵ_{Nd} values of geologic units and major rivers of the Himalaya,
 828 Tibet and Myanmar domain

Potential Source	$^{87}\text{Sr}/^{86}\text{Sr}$	ϵ_{Nd}	References
<i>Himalaya and Tibet domain</i>			
Lesser Himalaya	0.72–0.94	-25.3 to -23.5	Singh et al. (2008) and references therein
Greater Himalaya	0.73–0.79	-18 to -13.6	Singh and France-Lanord (2002); Singh et al. (2008) and references therein
Tethyan Himalaya	0.71–0.73	-15 to -12	Singh et al. (2008) and references therein
Gangdese arc (volcanics and granitoids in the southern Lhasa block)	0.70–0.73	-9 to +6	Wu et al. (2010) and references therein
<i>Myanmar domain</i>			
Paleogene Indo-Burman Ranges	0.714–0.716	-8.6 to -4.0	Colin et al. (1999); Allen et al. (2008)
Burmese arc (Wuntho-Popa Arc and intrusive rocks in Mogok Metamorphic Belt)	0.70–0.73	-10 to +4	Lin et al. (2019)
<i>Major Rivers</i>			
Ganges River (mainstream)	0.748–0.787	-21.3 to -15.7	Singh et al. (2008)
Brahmaputra River (mainstream)	0.718–0.749	-16.9 to -12.5	Singh and France-Lanord (2002)
Irrawaddy River	0.713–0.714	-8.3 to -10.7	Colin et al. (1999); Allen et al. (2008)

829 * All the ϵ_{Nd} values and $^{87}\text{Sr}/^{86}\text{Sr}$ ratios are recalculated at time T=0.

830

831 **Appendix A. Supplementary materials**

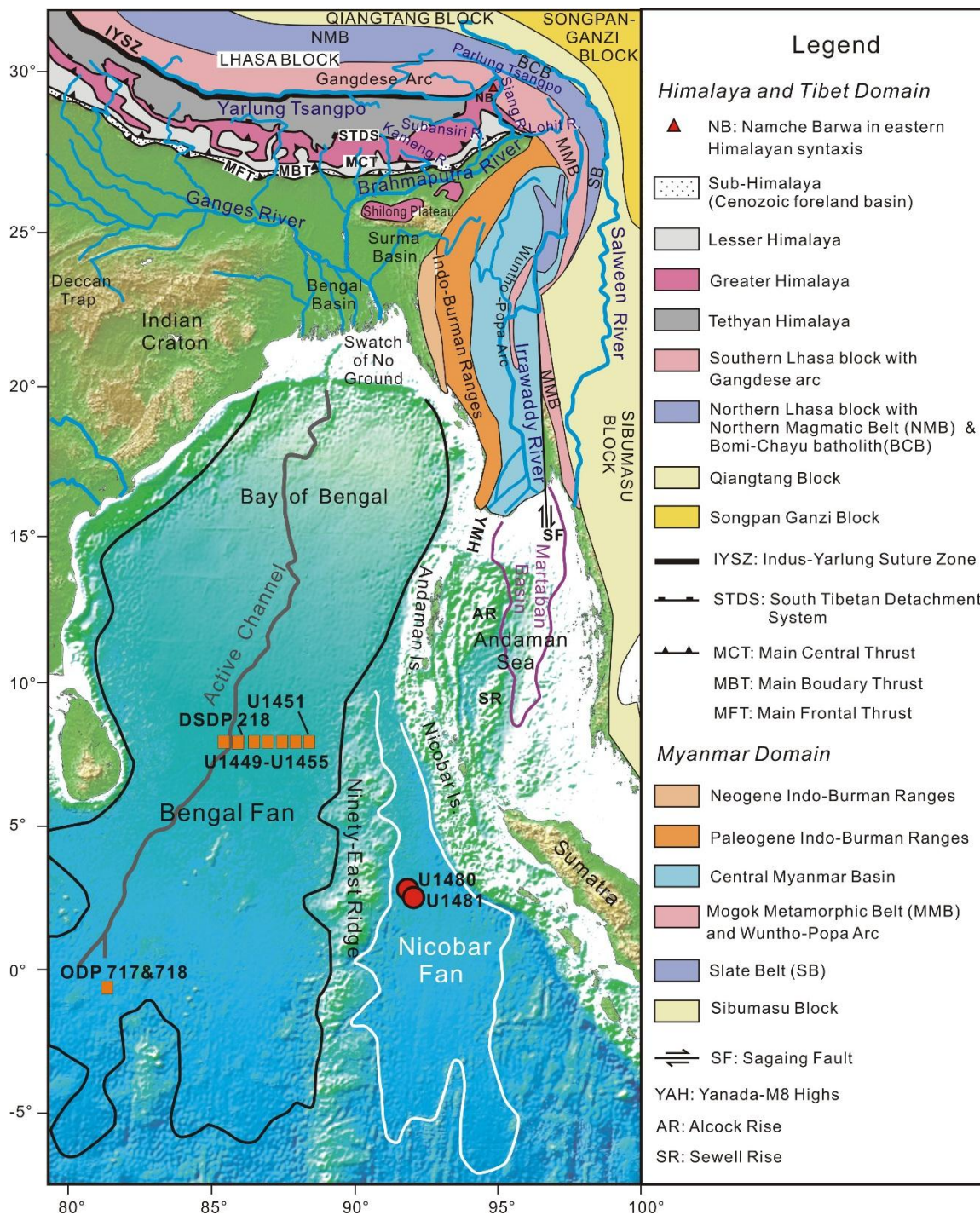
832 Full Analytical Method

833 Table A.1. Trace elements of the Nicobar Fan sediments

834 Table A.2. Sr-Nd isotope composition of the Nicobar Fan sediments

835 Fig. A.1. Cr/Th versus Th/Sc diagram for the Nicobar Fan sediments

836



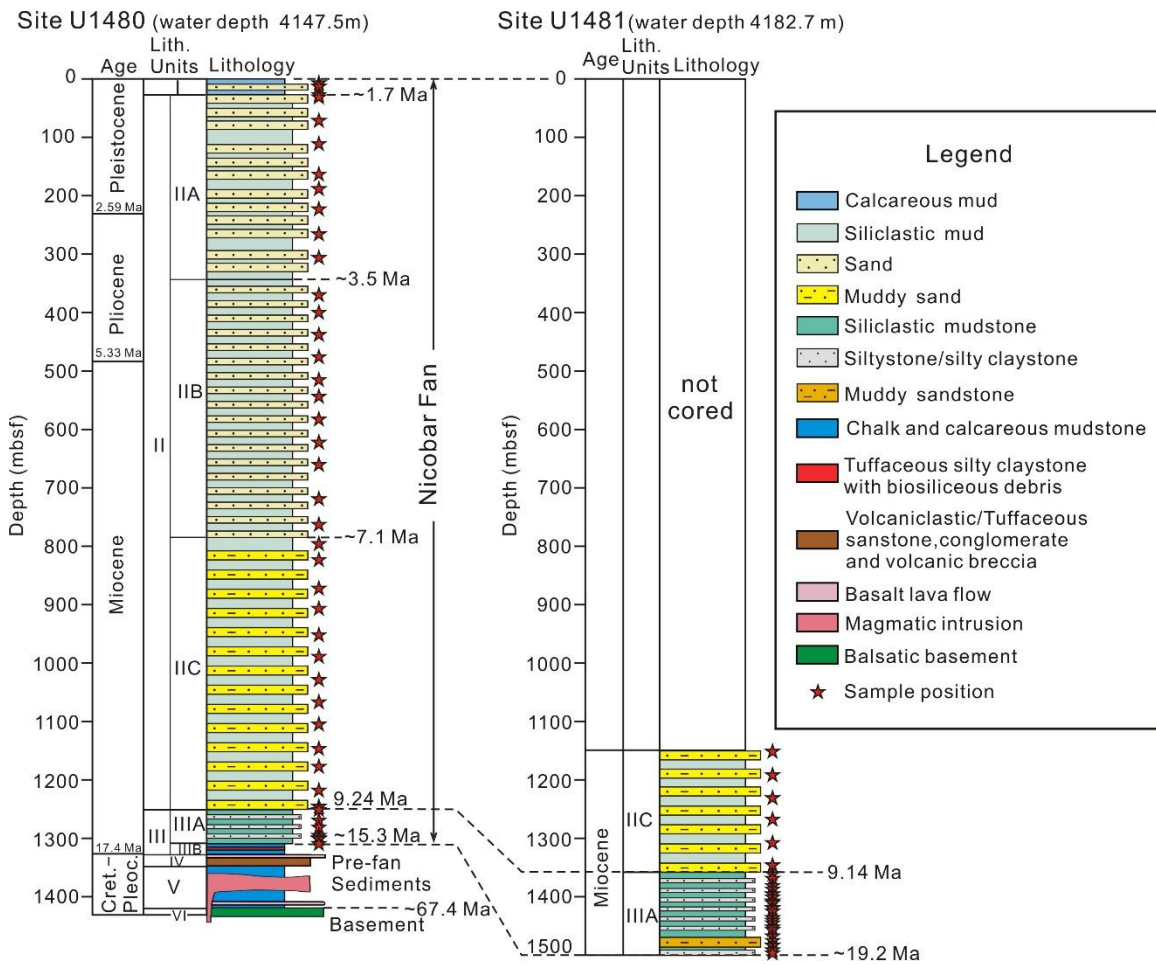
837

838

Fig. 1

839

840

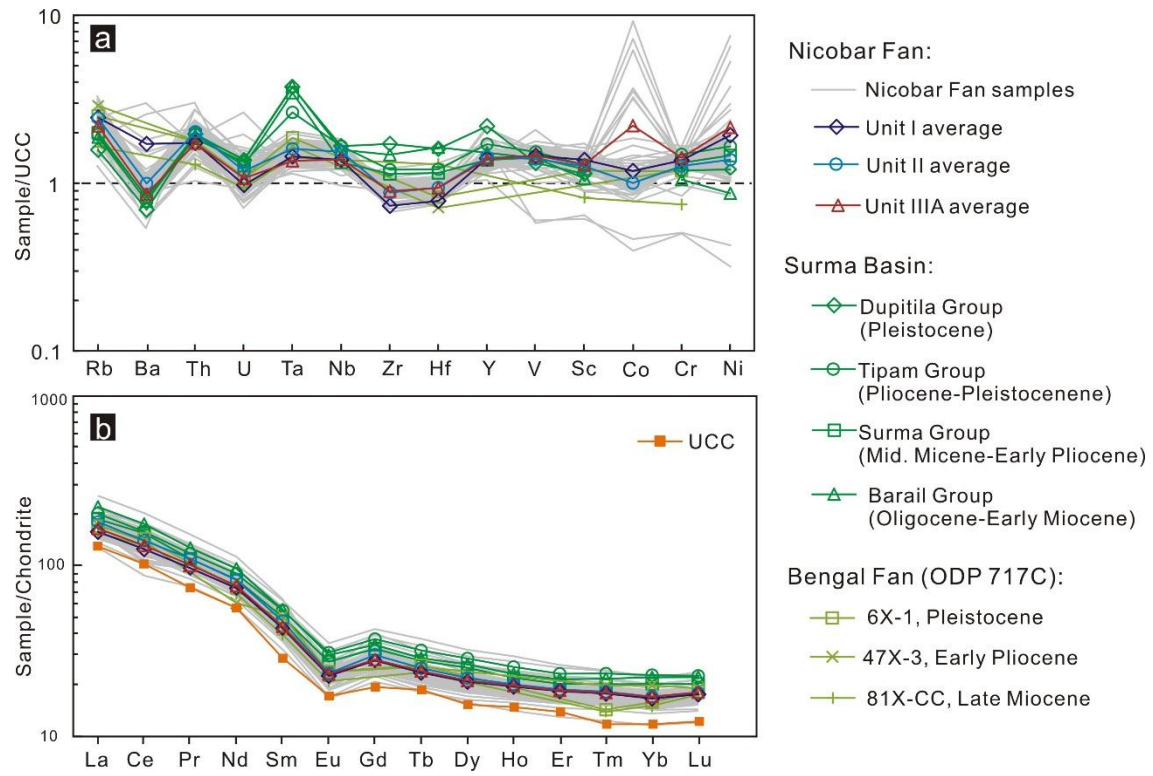


841

842

843

Fig. 2

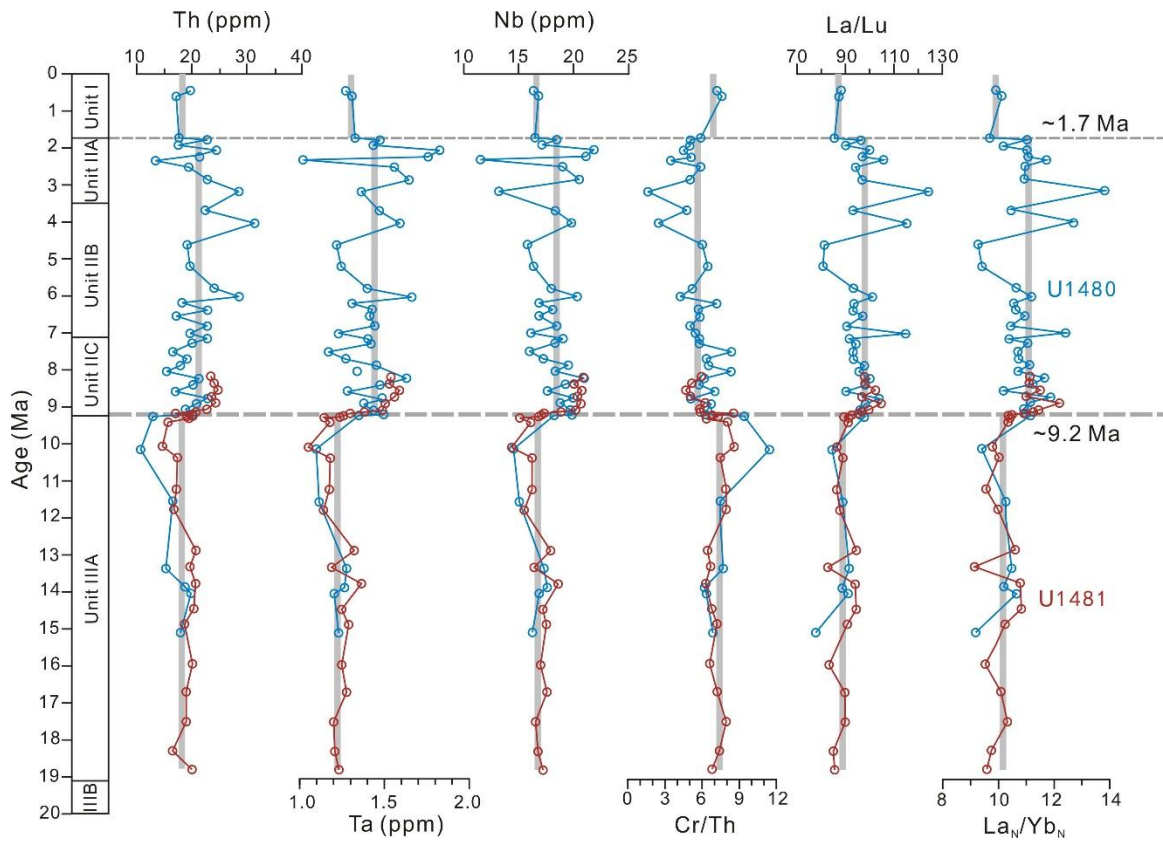


844

845

Fig. 3

846

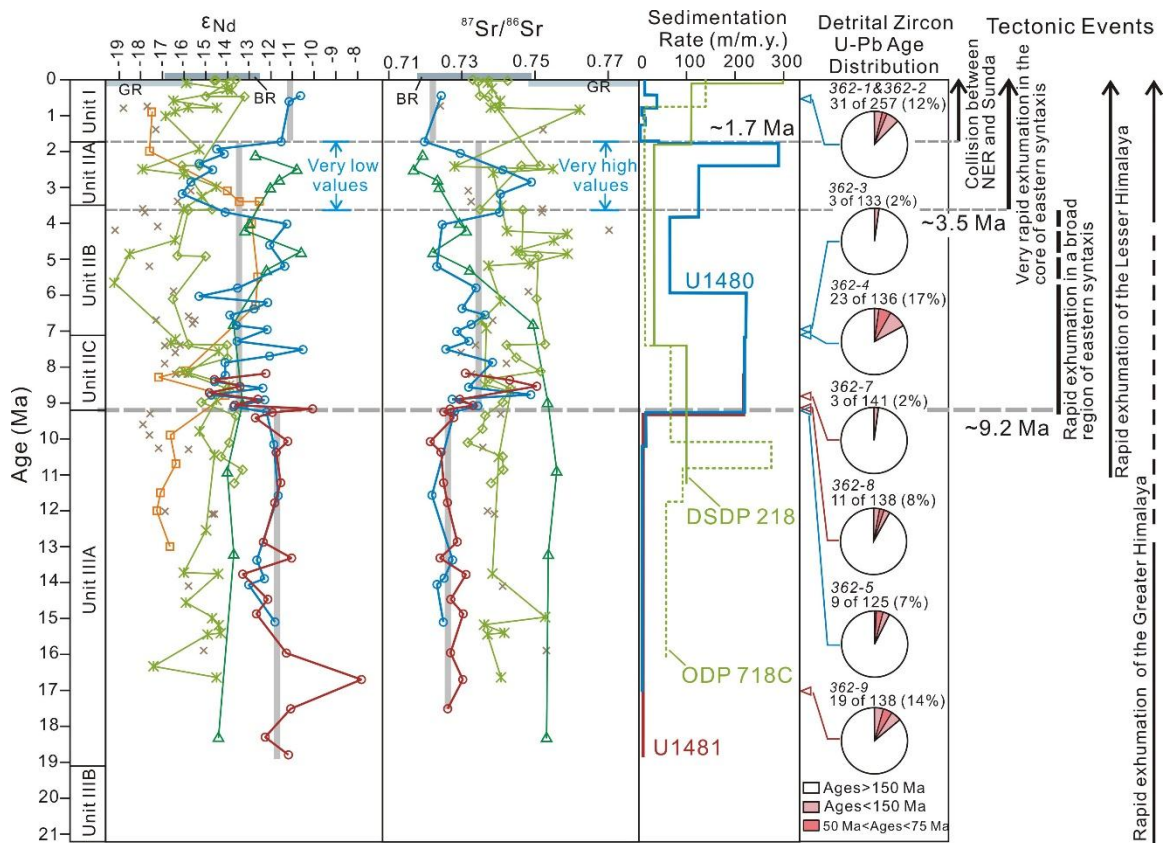


847

848

Fig. 4

849



Legend

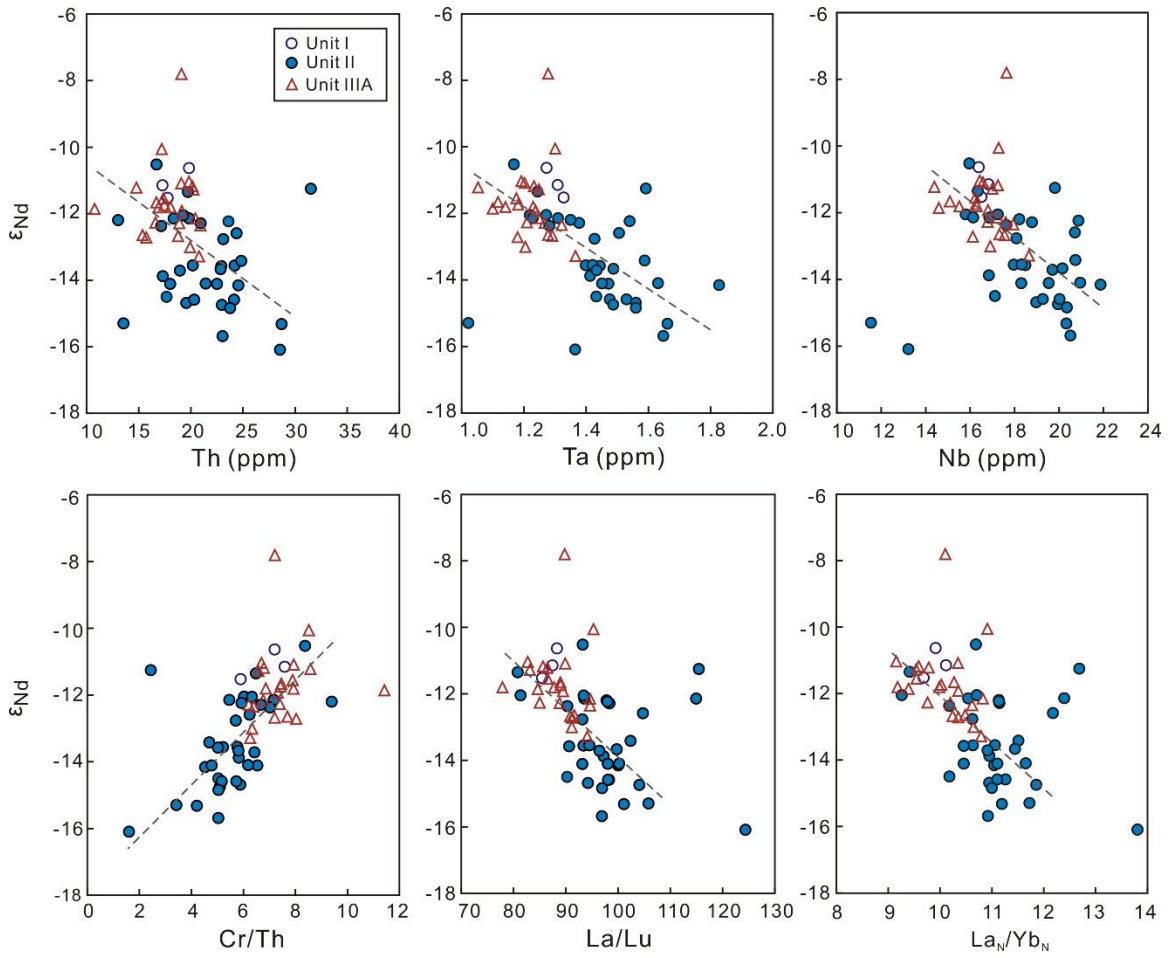
- U1480, Nicobar Fan
- U1481, Nicobar Fan
- *— ODP 717C&718C, Bengal Fan(France-Lanord et al., 1993; Galy et al., 1996)
- *— DSDP 218, Bengal Fan(Galy et al., 2010)
- △— Surma Basin (Bracciali et al., 2015)
- Eastern Himalaya foreland (Kameng River section, Chirouze et al., 2013)
- × Nepalese foreland (Huyghe et al., 2001, 2005; Szulc et al., 2006)
- Bramaputra River (Singh and France-Lanord, 2002)
- Ganges River (Singh et al., 2008)

850

851

Fig. 5

852



853

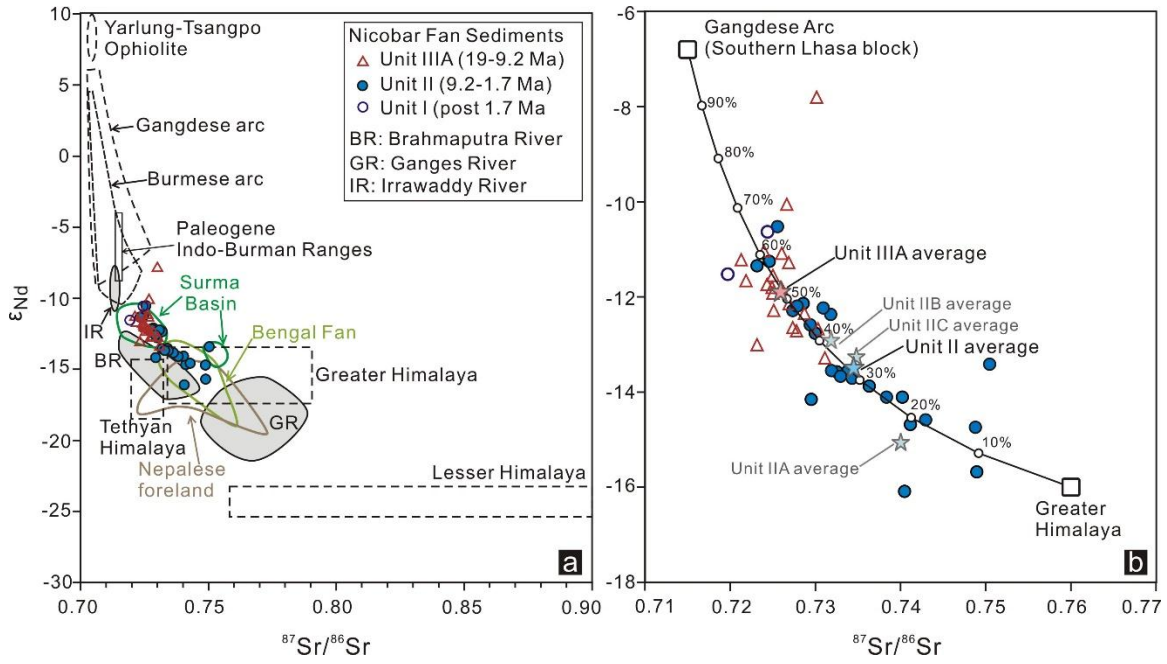
854

855

856

Fig. 6

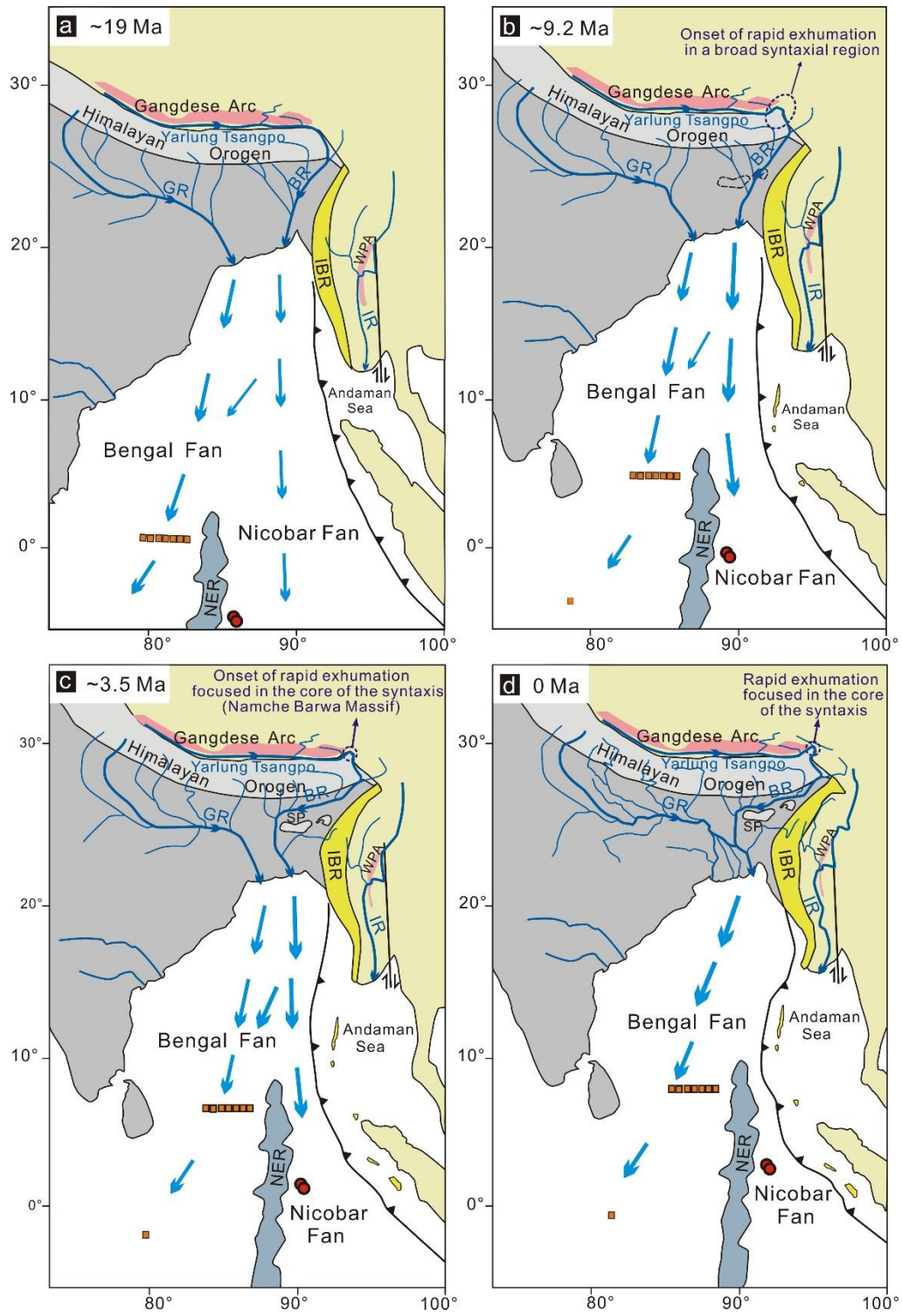
857



858

859

Fig. 7



860

861

Fig. 8

862